

MIRA VARIABLE STARS FROM LAMOST DR4 DATA: EMISSION FEATURES, TEMPERATURE TYPES, AND CANDIDATE SELECTION

YUHAN YAO¹, CHAO LIU², LICAI DENG², RICHARD DE GRIJS^{1,3}, AND NORIYUKI MATSUNAGA⁴

¹Kavli Institute for Astronomy & Astrophysics and Department of Astronomy, Peking University, Yi He Yuan Lu 5, Hai Dian District, Beijing 100871, China

²Key Laboratory for Optical Astronomy, National Astronomical Observatories, Chinese Academy of Sciences, 20A Datun Road, Chaoyang District, Beijing 100012, China

³International Space Science Institute–Beijing, 1 Nanertiao, Hai Dian District, Beijing 100190, China

⁴Department of Astronomy, The University of Tokyo, 7-3-1 Hongo, Bunkyo-ku, Tokyo 113-0033, Japan

Submitted for publication in The Astrophysical Journal Supplement Series

ABSTRACT

Based on an extensive spectral study of a photometrically confirmed sample of Mira variables, we find a relationship between relative Balmer emission-line strength and spectral temperature of O-rich Mira stars. The $F_{H\delta}/F_{H\gamma}$ flux ratio increases from less than unity to five as stars cool down from M0 to M10, which is likely driven by increasing TiO absorption above the deepest shock-emitting regions. We also discuss the relationship between the equivalent widths of the Balmer emission lines and the photometric luminosity phase of our Mira sample stars. Using our 291 Mira spectra as templates for reference, 191 Mira candidates are newly identified from the LAMOST DR4 catalog. We summarize the criteria adopted to select Mira candidates based on emission-line indices and molecular absorption bands. This enlarged spectral sample of Mira variables has the potential to contribute significantly to our knowledge of the optical properties of Mira stars and will facilitate further studies of these late-type, long-period variables.

Subject headings: catalogs — stars: AGB and post-AGB — stars: late-type — stars: statistics — surveys

1. INTRODUCTION

Mira stars are a class of late-type, long period variables (LPVs) that coincide with the coolest, most luminous part of the asymptotic giant branch (AGB). The AGB is the final stellar evolutionary phase of low- to intermediate-mass (1–8 M_{\odot}) stars before the envelope ejection phase (Habing & Olofsson 2003). Miras are, by definition, AGB variable stars exhibiting large luminosity amplitudes (>2.5 mag in the V band) with periods in excess of 80 days.

Just like other AGB giants, Miras can be divided into M-, S-, and carbon N-type stars. The differences among these groups are defined in terms of the relative abundances of oxygen and carbon in their photospheres. In M-type stars, a small amount of carbon in the stellar atmosphere is largely consumed by carbon monoxide (CO), so there is surplus oxygen left to form molecules such as TiO. During the thermally pulsating AGB (TP-AGB) phase, s-process elements (e.g., ZrO) and carbon from deep inside the star can be dredged up to the surface in stars with sufficiently large initial masses. Stars containing both TiO and ZrO are known as MS stars. As a star evolves up the AGB, the dredge-up continues to enrich the stellar envelope, so more carbon soaks up all excess oxygen into CO, leading to pure S or SC stars. Further enrichment brings up plenty of carbon to form C₂, CN, and/or CH molecules, which dominate the spectra of carbon N-type stars (Habing & Olofsson 2003; Green 2013; Van Eck et al. 2017). As soon as the C/O ratio increases to above unity, the difference in chemical composition leads to a significant decrease in the effective temperature, T_{eff} (Marigo et al. 2008).

Based on extensive observations of Mira stars since the

1940s, it has been found that one of the major spectral characteristics of these stars resides in their high-excitation emission lines. These lines vary over the pulsation cycle, but they are strongest around maximum light and weakest after minimum luminosity (Gray & Corbally 2009). Shock-heating of the atmosphere is verifiably at the basis of these variations (Deutsch & Merrill 1959; Gorbatskii 1961; Willson 1976; Fadeyev & Gillet 2004).

For O-rich Miras, the emission-line flux of H δ is greater than that of H γ , which, in turn, is greater than that of H β ; H α is weakest among the four lines in Balmer series. This so-called ‘Balmer increment’ is not found in C-rich stars, which show the opposite behavior (Merrill 1940). This tendency for O-rich Miras was initially attributed to obscuration by overlying absorption (Merrill 1945; Joy 1947). Luttermoser & Bowen (1992) subsequently proposed that non-local thermal equilibrium (NLTE) radiative transfer on its own can also give rise to the phenomenon. However, their interpretation, based on Bowen (1988)’s models, assumed the existence of an extended chromosphere, which does not exist in real Mira variables. Instead, it is only the innermost shock region that produces the observable Balmer-line emission (Fox et al. 1984; Richter et al. 2003).

Apart from the hydrogen Balmer series, many metallic emission lines, such as MgI, MnI, SiI, FeI, and FeII, as well as forbidden [FeII] emission lines, are also reported for M-type Mira stars. However, metallic emission lines appear late in the pulsation cycle, and vary independently of the hydrogen lines (Joy 1954; Richter & Wood 2001; Giridhar 2010).

Mira variables have long been used as tracers of stellar populations, because they are visible beyond the Local Group (Rejkuba 2004). Although Mira period–

luminosity (PL) relations exhibit an intrinsic dispersion in the optical (de Grijs 2011), it has been found that such dispersions are smaller at near- and mid-infrared (IR) wavelengths for Miras with thin dust shells and periods of less than 400 days (Whitelock et al. 2008; Matsunaga et al. 2009; Whitelock 2013). Thus, their PL relations can be used to trace the structure of the Milky Way (MW) galaxy and beyond (Catchpole et al. 2016; López-Corredoira 2017). Moreover, SiO masers from Mira stars have proved powerful tools for investigating stellar motions in optically obscured regions of the MW (Fujii et al. 2006; Deguchi et al. 2007, 2008, 2010; Deguchi 2012). Stepping into the *Gaia* era, a first result from *Gaia* Data Release 1 (DR1) used Miras to probe the outer regions of the Large Magellanic Cloud (Deason et al. 2017). Therefore, increasing the number of either type of Mira stars would be very helpful for similar future studies.

Generally, the study of Mira stars involves both long-term IR photometric and carefully planned spectroscopic observations. Therefore, for years optical spectroscopy of Mira stars has focused on well-known targets. Thanks to the wide-field Large sky Area Multi-Object fiber Spectroscopic Telescope (LAMOST) survey, we now have a chance to perform a novel, comprehensive study of Mira variables, investigate their overall optical spectral properties, and provide insights into the physical mechanisms driving these late-type stars.

This paper is organized as follows. A brief introduction to the LAMOST survey and the sources of our photometrically confirmed Mira sample are given in Section 2. In Section 3, we provide a detailed description of our template Mira spectra, discuss new observational phenomena, and suggest possible stellar processes for interpretation. In Section 4, we outline the method used to search for Mira candidates in the LAMOST catalog. A discussion and conclusions of this work are given in Section 5.

2. DATA

2.1. LAMOST

LAMOST is a 4 m-diameter reflective Schmidt telescope equipped with 4000 fibers in its focal plane, allowing it to obtain spectra covering the wavelength range from 380 to 900 nm at a spectral resolution of $R = 1800$ (Zhao et al. 2012; Cui et al. 2012). The five-year General Survey of LAMOST (2012–2017) is mainly a Galactic stellar survey. As a major component, the ‘LAMOST Experiment for Galactic Understanding and Exploration’ (LEGUE) survey has been designed to target a uniform and (statistically) complete sample of all stellar populations (Deng et al. 2012). Therefore, Miras, as evolved AGB stars, are included in its observations.

By the end of March 2016, the LAMOST DR4 catalog had accumulated 7,681,185 spectra, of which 6,898,298 were of stars. These 1D spectra have been processed by the LAMOST data reduction system. Basic reduction steps such as de-biasing, flat-fielding, fiber tracing, sky subtraction, and wavelength calibration are included in its 2D pipeline. Absolute flux calibration has not been done. However, relative flux calibration was performed (in terms of the flux per unit wavelength) by selecting stars with high-quality spectra as standard stars. Using a cross-correlation method, the 1D pipeline assigns a spectral type and redshift to each 1D spectrum (Luo et

TABLE 1
LINE INDEX DEFINITIONS

Name	Index Bandpass (Å)	Shoulder Bandpass(es) (Å)
H δ	4096–4109	4085–4094, 4112–4122
Fe4202	4197–4208	4183–4192, 4208–4217
Fe4308	4304–4314	4291–4302, 4315–4323
H γ	4332–4347	4320–4332, 4349–4352
Fe4376	4370–4382	4361–4370, 4383–4392
Mg4571	4567–4576	4556–4566, 4578–4584
H β	4857–4868	4845–4855, 4875–4880
H α	6548–6578	6505–6540, 6580–6610
CaH2	6814–6846	7042–7046
CaH3	6960–6990	7042–7046
TiO5	7126–7135	7042–7046

al. 2012, 2015).

In this paper, we measure the spectral indices of LAMOST spectra. The relevant wavelength ranges of the indices and their shoulder bandpass(es) are included in Table 1. The definitions of the line indices, in terms of their integrated flux (F ; Section 3.2.1), equivalent width (EW; Sections 3.4, 4.3, and 4.4), and the band indices (R_{ind} ; Section 4.2) will be included when they are first used in the text.

2.2. A Photometrically Confirmed Sample

We compiled a photometrically confirmed sample of Mira variables from the Kiso Wide-Field Camera (KWFC) Intensive Survey of the Galactic Plane (KISOGP) (Matsunaga 2017), the American Association of Variable Star Observers (AAVSO) International Database Variable Star Index (VSX; Watson 2006, version 2017-05-02; we selected stars of variability type ‘M’), and the SIMBAD Astronomical Database.

The KISOGP survey uses the KWFC mounted on the 105 cm Schmidt telescope at Kiso observatory, Japan. Having obtained I -band photometric measurements of $m_I = 9.5$ – 16.5 mag, from 2012 to 2015, this survey identified more than 700 Mira stars in the northern Galactic disk with periods between 100 and 600 days, of which roughly 90% were newly found.

We first cross-matched the KISOGP and VSX Miras with the LAMOST DR4 catalog. Spectra that suffer from serious contamination by sky lines, low signal-to-noise ratios (SNRs), flux saturation, or which display characteristics of a binary spectrum were excluded from the Mira sample. This resulted in 19 and 238 spectra for, respectively, KISOGP and VSX targets. (Eight spectra were in common between the VSX and KISOGP catalogs; they were only included among the 19 spectra with KISOGP designations.)

For KISOGP targets, the period and epoch (date of light maximum) were calculated from the KISOGP light curves using generalized Lomb Scargle (GLS) fitting (Zechmeister & Kürster 2009), which is a common approach to estimate the sinusoidal primary frequency. The phases of each spectrum were calculated using

$$\phi = \frac{(\text{observed date} - \text{epoch}) \bmod \text{period}}{\text{period}} \quad (1)$$

As regards VSX targets, if period or epoch information was available in the VSX catalog, we estimated the phase using Eq. (1), and adopted the resulting value if

$$\frac{\text{observed date} - \text{epoch}}{\text{period}} < 18 \quad (2)$$

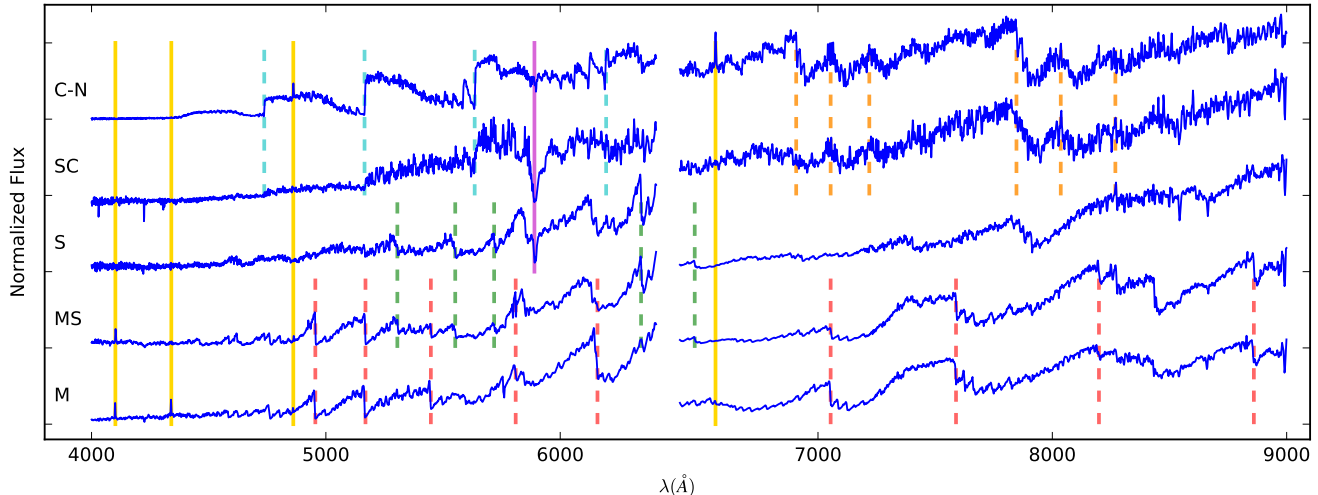


FIG. 1.— (bottom to top) The M \rightarrow MS \rightarrow S \rightarrow SC \rightarrow C spectral sequence of LAMOST Mira spectra. Each spectrum is normalized at both 6315Å and 8750Å. Solid lines indicate emission-line wavelengths (yellow: Balmer series; purple: NaI D doublet). Dashed lines indicate band heads of molecular absorption bands (red: TiO; green: ZrO; cyan: C₂; orange: CN).

to ensure accuracy. For targets without such information, we searched for their light curves in the Northern Sky Variability Survey¹ (Woźniak et al. 2004, NSVS) and the All Sky Automated Survey² (Pojmański 2014, ASVS). If available, we fitted the light curve and repeated the steps of Eqs (1) and (2).

Finally, we cross-matched the DR4 catalog with the SIMBAD database, because some Mira stars have a SIMBAD designation but are not included in the VSX or KISOGP catalogs. This procedure resulted in the identification of another 34 Mira spectra,³ resulting in a total number of 291 Mira spectra.

3. MIRA SPECTRA

3.1. Overview: the Spectral Sequence

Based on the TiO, ZrO, C₂ and CN molecular bands, we broadly divided the 291 Mira spectra into O-rich (258) and C-rich (33) Miras. Among the C-rich spectra, six are of type SC, which show no TiO, weak or no ZrO/C₂, and very strong D lines, as defined in the Boeshaar–Keenan System (Keenan & Boeshaar 1980). Among the O-rich spectra, about 20 are of types MS or S, which show prominent ZrO features. We show one spectrum of each type in Figure 1. The Balmer *decrement* in C-rich Miras ($F_{H\delta} < F_{H\gamma} < F_{H\beta} < F_{H\alpha}$) and the Balmer *increment* in O-rich Miras are also clearly seen.

Molecular dissociation calculations (Scalo & Ross 1976) have demonstrated that the sequence M \rightarrow MS \rightarrow S \rightarrow SC \rightarrow C represents an increase in the ratio of carbon to oxygen; this ratio passes through a value of unity in SC stars (Gray & Corbally 2009). The sample of LAMOST Mira spectra covers the entire evolutionary sequence of Mira variables in the TP-AGB phase.

3.2. O-rich

3.2.1. Balmer Emission in Subtypes

From among the 258 O-rich spectra, we selected 104 with observable Balmer emission(s), and assigned a temperature type to each of them by comparison with the LAMOST M0–M6 giant templates from Zhong et al. (2015, hereafter Z15), as well as the M0–M10 intrinsic templates derived by Fluks et al. (1994). From a careful comparison of these spectral templates, it follows that the Balmer increment relation only holds for late-type O-rich Miras (M5–M10). As for the early-type spectra, we see a Balmer *decrement* for M1 and M2, but H α is weak in the only M0 spectrum in our sample. We also observe nearly equivalent strength for the Balmer lines in the case of M3. For spectra later than M4, the strengths of H α and H β decrease and H δ becomes the strongest line.

We use the flux ratio of H δ and H γ to quantify this relationship, because they are visible for the longest duration. We define the integrated line flux as

$$F = \int (f_{\text{line}}(\lambda) - f_{\text{cont}}(\lambda)) d\lambda, \quad (3)$$

where $f_{\text{line}}(\lambda)$ is the flux of the spectral line in the relevant index bandpass (see Table 1) and $f_{\text{cont}}(\lambda)$ is the pseudo-continuum estimated through linear interpolation in the shoulder bandpass(es).

Box-and-whisker plots of $F_{H\delta}/F_{H\gamma}$ for each subtype are shown in Figure 2, with the background yellow histogram indicating the number of spectra used for each subtype. Our sample is dominated by M5–M8. From M0 to M3 the ratio does not change much; it even decreases somewhat. The median inverts from ‘<1’ to ‘>1’ between M4 and M5. For spectra later than M5, the ratio increases. More M0–M4 and M9–M10 templates are needed to render this relation more accurate. From Figure 2, we are aware of the large intrinsic variance within each type, so this relationship cannot be used individually to assign spectral types to optical spectra.

Early observations by Merrill (1945) of bright Mira stars revealed that the low intensities of H α , H β , and H γ are mainly owing to absorption by TiO molecular bands. These overlapping absorptions originate above the deepest shock layer, and they can thus effectively

¹ <http://www.skydot.lanl.gov/nsvs/nsvs.php>

² <http://www.astrow.edu.pl/asas/?page=aasc>

³ 24 of them are also tabulated in the VSX, 22 of which are semi-regular variables and the other two are marked as long-period variables.

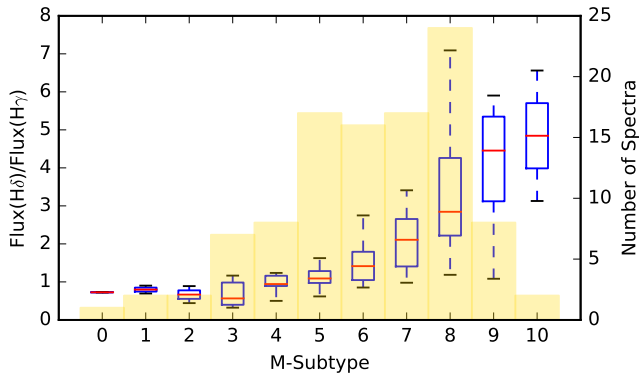


FIG. 2.— Box-and-whisker plot of the $F_{H\delta}/F_{H\gamma}$ ratio for each subtype of O-rich Mira templates. The box extends from the lower to upper quartile values, with a red line at the median. The whiskers extend from the box to show the range of the data. The yellow histogram indicates the number of spectra used for each subtype.

block radiation from internal atmospheric layers where the Balmer lines are formed (Siviero et al. 2016). Our result agrees well with this scenario: as an AGB star cools down from M0 to M10, the TiO bands strengthen gradually, so more flux is absorbed by the lower-order Balmer lines, leading to an increase in $F_{H\delta}/F_{H\gamma}$. Note that narrow portions of H δ and H γ are sometimes absorbed by superimposed metal lines of iron, vanadium, yttrium, and indium (Adams 1941; Joy 1947), but this effect has little influence on the overall integrated flux of low-resolution spectra.

Also note that all five M0–M2 spectra in our O-rich sample have strong Balmer lines, regardless of our knowledge that the emission strengths are strongly correlated with luminosity phase.

3.2.2. Metallic Emission

Among the 258 O-rich sample stars, we can distinguish four metallic lines in 20 spectra, as shown in Figure 3. The emission lines are Fe I $\lambda\lambda$ 4202, 4308, 4376 and Mg I 4571, all of which are well-known emission features of Mira stars (Gray & Corbally 2009). We note that 17 of the 20 spectra are of types M8–M10, with M5 being the earliest type. This is a strong indication that these four emission lines are mostly developed in late-type O-rich Miras.

3.3. C-rich Spectra

All of our C-rich spectra are included in the Appendix (see Figure 11). The small number of C-rich sample stars, as well as the difficulty in finding a clean control sample of non-variable carbon N-type spectra, prevents us from carrying out a detailed study similar to what we did for our O-rich sample.

However, there are still two features of interest. First, more than half of the 33 spectra exhibit very strong H α emission, much stronger than the weak emission shown in Barnbaum et al. (1996, the Bambaum Atlas includes a sample of non-variable carbon N-type stars). Second, except for two SC-type stars, none of our C-rich sample spectra show the CaII $\lambda\lambda$ 8498,8542,8662 triplet.

3.4. Emission as A Function of Phase

We will next investigate the relationship between the Balmer emission strength and the corresponding luminosity phase, ϕ . Use of the flux-based definition of the line index, Eq. (3), is most appropriate when comparing fluxes of different lines based on a single spectrum, but here we need to characterize the emission strengths for all emission spectra in our sample. Hence, we use the EW (Worthey et al. 1994) as an indication of line strength. The EW is defined as

$$EW = \int \left(1 - \frac{f_{\text{line}}(\lambda)}{f_{\text{cont}}(\lambda)} \right) d\lambda, \quad (4)$$

where $f_{\text{line}}(\lambda)$ and $f_{\text{cont}}(\lambda)$ have the same meaning as in Eq. (3).

For spectra with low SNRs, fluxes in the shoulder bandpass(es) tend to be noisy, and thus the pseudo-continuum estimated through linear interpolation does not always represent the continuum level very well. Hence, we define a local SNR for every line index to quantify the significance of the measured EW. Using the concept of the inverse variance,

$$SNR_{\text{local}} = \frac{1}{\text{Var}(f_{\text{line}}(\lambda) - f_{\text{cont}}(\lambda))}, \quad (5)$$

where the definition domain of λ includes the shoulder bandpass(es). For a spectrum with $SNR > 20$, the typical uncertainty in the EW of an atomic line is less than 0.1 Å (Liu et al. 2015). Note that for emission lines the relevant EWs are negative, so the smallest value indicates the strongest line strength.

The measured emission-line indices were accepted if SNR_{local} was greater than 5, and the number of bad pixels in the index bandpass was zero. The resulting measurements are shown in Figure 4.

The top two panels show the EW as a function of ϕ for H δ and H γ . The general trend of ‘higher luminosity, stronger emission’ for O-rich Miras is consistent with many previous case studies (e.g., Fox et al. 1984; Fox & Wood 1985; de Laverny & Magnan 1995; Castella et al. 2000). The bottom two panels clearly show that the C-rich Miras exhibit stronger emission in lower-order lines and particularly much greater variation in H β . Mikulášek & Gráf (2005) showed that for C-rich Miras, the H α EW is also strongly correlated with photometric phase. This can also be seen in the bottom right-hand panel of Figure 4.

Our limited sample is based on observations of different stars over different pulsation cycles, and it is thus not accurate enough to derive strict relations. However, it can provide an approximate test of how LAMOST spectra can support previous studies and provide us with information regarding which emission lines should be measured for the identification of O- and C-rich Mira candidates. Moreover, LAMOST has been scheduled to observe more KISOGP Miras, whose spectra will allow us to better constrain phases of light minima (or maxima), with higher precision. These data will allow us to provide a more secure treatment of the interaction between the propagation of shock waves and the stars’ pulsations.

4. CANDIDATE SELECTION

In this section, we select possible Mira stars from the LAMOST DR4 catalog. We are motivated to do so with

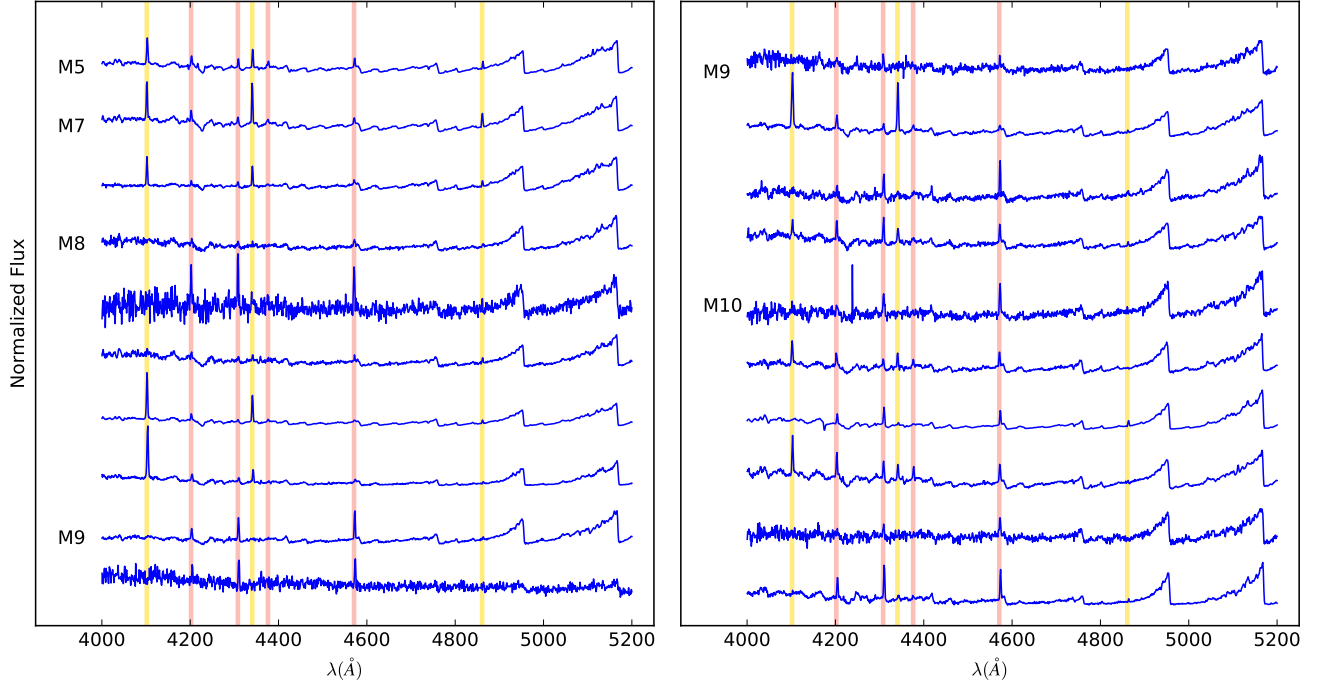


FIG. 3.— Twenty O-rich templates with metallic emission normalized at 5175 Å. Colored lines indicate the emission wavelength (yellow for Balmer lines; pink for metallic lines).

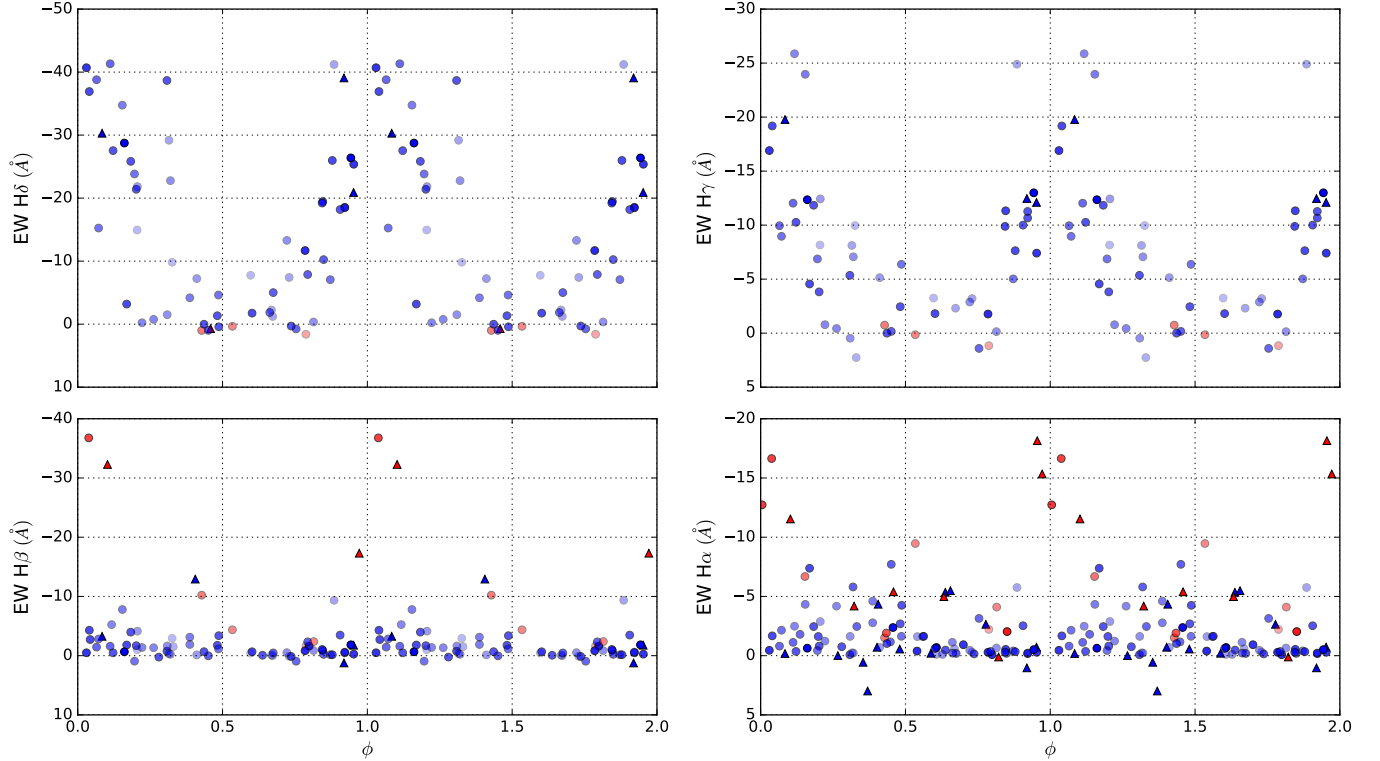


FIG. 4.— Balmer emission strength (EW) as a function of pulsation phase (ϕ). O- and C-rich spectra are plotted in blue and red, respectively. Triangles and circles are KISOGP and VSX targets, respectively. For phases calculated from VSX data and NSVS/ASVS light curves, we use variations in transparency to indicate the accuracy (the deeper the color, the smaller the value of Eq. 2).

TABLE 2
SUBCLASSES OF OUR MIRAS SAMPLE
IDENTIFIED BY THE LAMOST 1D PIPELINE

Type	Total	M	Non ^a	Carbon
Oxygen-rich	258	219	38	1 ^b
Carbon-rich	33	1 ^c	5	27

^a Failure to identify a subclass.

^b This is a type-M9 spectrum, misclassified as a result of the small number of late-type M-giant templates.

^c This is an SC-type star, misclassified as a result of the absence of S-star templates.

the expectation that such an inquiry may lead to the discovery of a large number of Mira candidates. The key steps are pre-selection based on photometric data, followed by spectral-line measurements.

4.1. Pre-selection

4.1.1. SNR Cut

Based on the notion that Miras have stronger fluxes at red wavelengths, we found the *i*-band *SNR* > 20 to be a good diagnostic of high-quality Mira spectra. All of our 291 templates meet this criterion.

4.1.2. Header Subclass

As outlined in Section 2.1, every LAMOST spectrum has a spectral type assigned to it by the LAMOST 1D pipeline (Luo et al. 2015). This pipeline produces four primary classes, i.e., star, galaxy, qso, and unknown. Within the ‘star’ class, the ‘subclass’ keyword provides a more detailed subtype. For galaxies, quasars, or unknown objects, this keyword is set to ‘Non.’ To test the accuracy of the pipeline for Mira stars, we found that all of our sample objects were included in the ‘star’ or ‘unknown’ classes; the associated subclasses are included in Table 2.

Given that 257 of the 258 (99.6%) O-rich Mira templates are identified as ‘M’ or ‘Non,’ we selected the 311,867 spectra of these two subclasses as our O-rich Mira candidates. Although the automated pipeline is not sufficiently efficient in classifying carbon stars, Ji et al. (2016) already identified 108 N-type carbon stars in the LAMOST DR2 catalog, and Y. B. Li et al. (in prep.) identified 266 N-type carbon stars in the DR4 catalog using different techniques.⁴ We included the results of these two studies and retrieved a total of 328 carbon stars, which were then combined with the 2184 spectra marked as ‘Carbon Star’ by the LAMOST pipeline. We subsequently removed all known Mira spectra from this database, yielding a total candidate number of 313,810.

4.1.3. 2MASS Cuts

Next, these Mira candidates were mapped onto the K_s versus $J - K_s$ plane. J and K_s magnitudes were obtained through cross-identification with the Two Micron All-Sky Survey (2MASS) all-sky point source catalog (Skrutskie et al. 2006). Only those stars with good photometric data (an ‘A’ quality flag in the J and K_s bands, i.e., 306,072 spectra) are shown in Figure 5. Among the 291 Mira

⁴ 57 of the 266 carbon stars come from the LAMOST pilot survey; they are not included in the DR4 catalog.

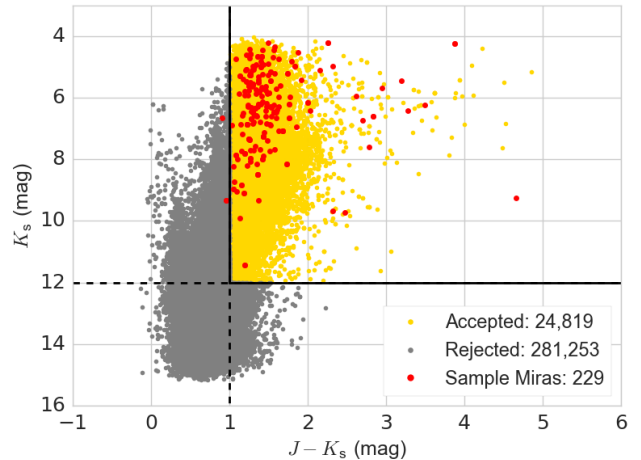


FIG. 5.— 2MASS color–magnitude diagram in the K_s vs. $(J - K_s)$ plane. The red dots represent template Mira stars, while yellow and gray dots represent accepted and rejected candidates, respectively. The solid black lines of $J - K_s > 1$ mag and $K_s < 12$ mag illustrate the criteria adopted to select Mira candidates.

templates, 229 Miras with high-quality 2MASS photometry are also included in the same plot. In Figure 5, 99.1% of the templates are sufficiently cool to be characterized by the empirical colors of giant stars, $J - K_s > 1$ mag (Wiśniewski et al. 2011), as well as bright, $K_s < 12$ mag. Two outliers with $J - K_s < 1$ are relatively bluer O-rich Miras. Therefore, by applying careful cuts in the color–magnitude diagram, we can remove most of the possible contaminants, leaving 32,557 (24,819 accepted plus 7738 without good 2MASS data) candidates.

4.1.4. SIMBAD Data

Finally, these candidates were cross-matched with the SIMBAD database; 1064 objects have SIMBAD designations that rule out a possible Mira nature, thus leaving us with 31,493 candidates. In this step, we also collected 197 spectra of known young stellar objects (YSOs) and T Tauri stars (TTS), both of which are types of pre-main-sequence dwarf stars. Their spectra will also be used in the next step.

4.2. Selection of M Giants

Contamination among the 30,248 O-rich candidates occurs mainly in the form of M dwarfs and ‘Non’-marked spectra of other types. Mann et al. (2012) showed that molecular band indices of CaH2, CaH3, and TiO5 are good gravity indicators for the determination of giant and dwarf luminosity classes. Introduced by Reid et al. (1995), band indices are calculated using the ratio of the average flux over the specified wavelength range, i.e.,

$$R_{\text{ind}} = \frac{\langle f_{\text{index}} \rangle}{\langle f_{\text{shoulder}} \rangle}. \quad (6)$$

Here, $\langle f_{\text{index}} \rangle$ and $\langle f_{\text{shoulder}} \rangle$ are the mean fluxes of all pixels in the index bandpass and the shoulder bandpass defined in Table 1, respectively. R_{ind} is a unitless number between 0 and 1. It decreases as the absorption becomes stronger.

We map each candidate spectrum associated with a real value⁵ for the line index onto the CaH2+CaH3 ver-

⁵ 191 of the measured indices are ‘infinity’ or ‘not a real num-

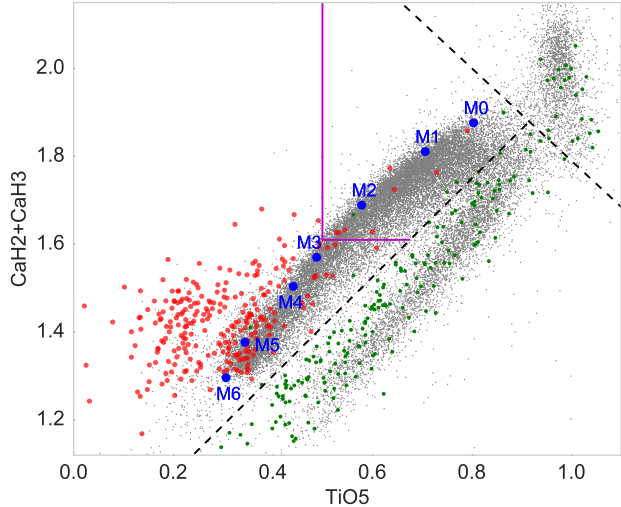


FIG. 6.— Distribution of candidates (gray), Miras (red), M-giant templates from Z15 (blue), YSO and TTSs (green) spectra in the CaH2+CaH3 versus TiO5 diagram. The black dashed lines represent Eqs (7) and (8), which are used to select 21,989 O-rich candidates and reject 8558 other candidates. The magenta lines represent Eqs (9) and (10).

sus TiO5 plane in Figure 6. Also included are the 258 O-rich templates (red) and the M0–M6 normal M-giant templates (blue) of Z15. Band indices of early-type giant stars are larger than those of late-type giants.

Ishihara et al. (2011) showed that some TTSs and YSOs have colors similar to O- or C-rich AGB stars. In addition, the optical spectra of M-type YSOs and TTSs (Saffe et al. 2003; Herczeg & Hillenbrand 2014) also have strong Balmer emission lines. To test if the CaH2+CaH3 vs. TiO5 diagram can efficiently separate them from M giants, 197 spectra of YSO and TTSs (green) are shown in green.

Compared with M dwarfs, M giants are located in the top branch because of their weaker CaH molecular bands, and they are clearly distinguishable by a selection cut of

$$\text{CaH2} + \text{CaH3} > 1.125 \times \text{TiO5} + 0.85. \quad (7)$$

In the top right-hand region of Figure 6, a cluster of dots centered on ($\text{TiO5} = 1$, $\text{CaH2} + \text{CaH3} = 2$) do not have any CaH or TiO features and thus are not spectra of M-type stars. A small number of YSO and TTSs also reside in this region; these are F- or G-type stars. They should be excluded from our O-rich candidates by a selection cut of

$$\text{CaH2} + \text{CaH3} < -\text{TiO5} + 2.8. \quad (8)$$

After having applied the cuts of Eqs (7) and (8), the number of O-rich candidates has been reduced to 21,989. Most TTSs and YSOs are excluded by application of the two cuts.

Following the distribution of M0–M6 templates, we roughly separated the accepted 21,989 candidates into 12,719 early- and 9270 late-type giants using cuts of

$$\text{CaH2} + \text{CaH3} > 1.61 \quad (9)$$

and

$$\text{TiO5} > 0.50. \quad (10)$$

ber,’ which are the results of bad pixels or corrupted spectra. We inspected these spectra by eye and rejected them as Mira spectra.

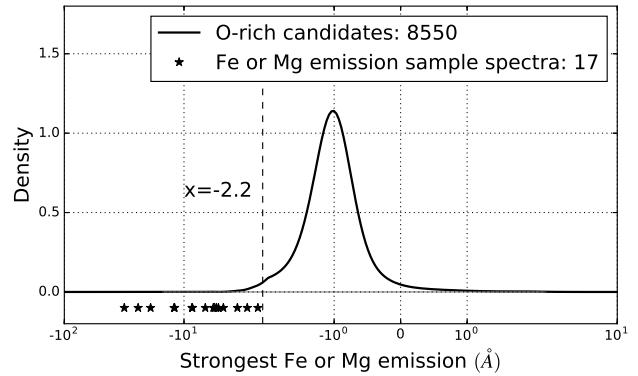


FIG. 7.— Distribution of The Strongest Emission EWs in Fe I $\lambda\lambda 4202, 4308, 4376$ and Mg I $\lambda 4571$. Kernel Density Estimation (KDE) with a Gaussian kernel is used for the visualization. X-axis values of the black asterisks at the bottom are EWs of all Fe and Mg emission template spectra.

The intention of this separation is to leave spectra of M5–M10 for the next step, i.e., the measurement of metallic lines, because based on Section 3.2.2, we do not expect such emission to be present in warm O-rich spectra. We intentionally adopted a flexible and wide limit (retaining M3–M10 instead of M5–M10), since we allow for contamination of early-type spectra in the late-type group.

4.3. Fe and Mg Emission

As suggested by Richter & Wood (2001, their Figure 23) and Gray & Corbally (2009, page 304), in O-rich Mira stars the metallic emission strength is not in phase with the Balmer strength. Therefore, before we measure the most commonly observed Balmer emission lines, line indices of Fe I $\lambda\lambda 4202, 4308, 4376$ and Mg I $\lambda 4571$ were measured to identify Mira spectra with Fe or Mg emission, which might not display Balmer lines.

Our candidates are the 9270 late-type O-rich spectra obtained in the previous step, and our templates are the 20 emission spectra shown in Figure 3. Using Eq. (4) as our definition of the EW and Eq. (5) to quantify the local SNR, we only accepted EWs if their SNR_{local} was no less than five, and if there was no bad pixel in the index bandpass, which means that we used the same criteria as those adopted in Section 3.4.

Figure 7 shows the probability density distribution of the strongest measured Fe or Mg EWs of our late-type, O-rich candidates. Here we choose the smallest value among the four measured line indices to single out the strongest emission. This might potentially bias the line indices to negative values for a given spectrum containing other spectral features or only noise across the measured wavelength range. Another potentially biasing effect is associated with an absorption band at 4582 \AA , near the right-hand shoulder of Mg I $\lambda 4571$, which might cause an artificial emission feature and systematically drive the measured value to become smaller. Therefore, the peak of the profile in Figure 7 is centered on minus one rather than zero.

Since all of the 20 Fe or Mg emission spectra⁶ among our templates have $\text{EW}(\text{Strongest Fe or Mg}) < -2.4 \text{ \AA}$, we adopted a cut at

$$\text{EW}(\text{Strongest Fe or Mg}) < -2.2 \text{ \AA} \quad (11)$$

⁶ 17 have ‘accepted’ strongest EWs.

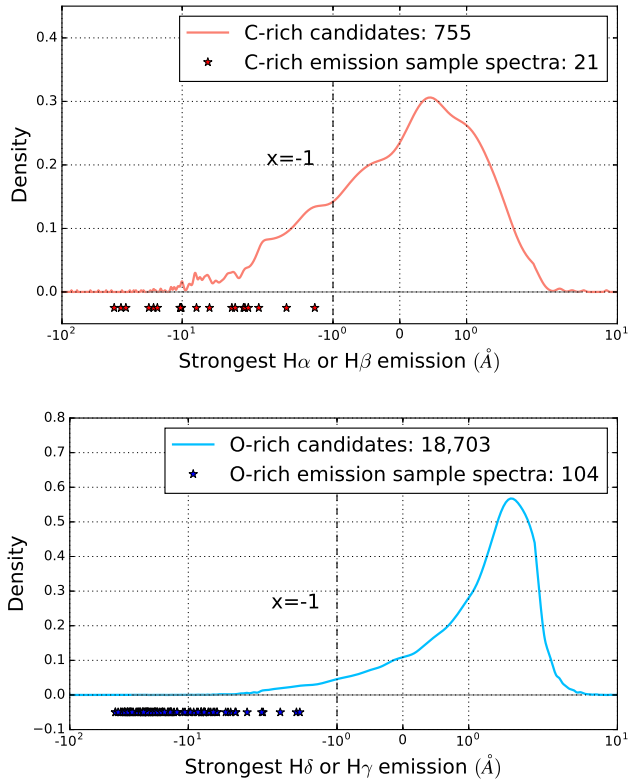


FIG. 8.— Top (bottom): Distribution of The Strongest Emission EWs in $H\alpha$ and $H\beta$ ($H\gamma$ and $H\delta$). The probability density distribution of C-rich (O-rich) candidates is shown by the KDE with a Gaussian kernel of 0.2 (0.1) times the bandwidth in the top (bottom) panel.

to select a sample composed of 338 candidates. We inspected the 338 spectra by eye. Most of their negative line indices are caused by noise. However, we also found 14 spectra in the range of M7–M10 that should be classified as Mira stars, as shown in the Appendix (see Figure 12). Three of these 14 spectra have prominent Fe or Mg lines (two with Balmer lines and one without), and the other 11 are classified based on the presence of hydrogen emission.

Now that we have successfully selected 14 Mira spectra, the number of O-rich candidates is reduced to 21,651.

4.4. Balmer Emission

EWs of hydrogen emission lines need to be measured to identify Mira spectra, see Eq. (4), Table 1. We chose to measure the first two lines in the Balmer series ($H\alpha$ and $H\beta$) for our 755 C-rich candidates, and the next two lines ($H\gamma$ and $H\delta$) for the 21,651 O-rich candidates. Again, we adopted the smallest value as an indication of the emission features. The acceptance criteria for every measurement are also the same as those adopted in Sections 3.4 and 4.3. However, this time we do not retain the ‘rejected’ spectra in our next step, because a high SNR value in the Balmer region is essential for identification of Mira spectra. Balmer emission template spectra (21 C-rich and 104 O-rich) were measured at the same time. A more plausible diagnostic might be found in measuring $H\alpha$ and $H\delta$ for C- and O-rich candidates, respectively. However, we measure two lines for each type, because if the SNR_{local} of one line is low, we could potentially still use the other. In addition, one C-rich template spectrum

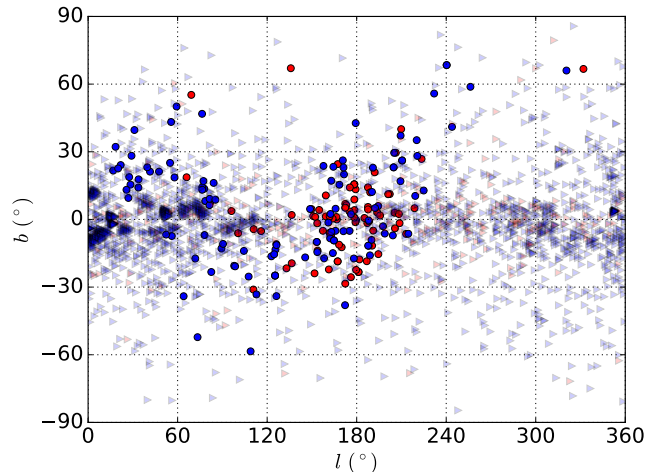


FIG. 9.— Galactic distribution of Mira stars. M- and C-type Mira variables are plotted in blue and red, respectively. Transparent triangular data points are Miras in the AAVSO VSX for which a designated SIMBAD type is available; circles are Miras identified in this paper. The concentration of a group of O-rich Miras around $l \sim 75^\circ$ is centered on the *Kepler* field.

only exhibits $H\beta$ emission (see Figure 11).

In each panel of Figure 8, the asterisk closest to zero is measured from a template spectrum whose Balmer emission can just be seen, and this can thus give us an upper limit to a distinguishable emission line. The peak of each profile is centered on a positive value, because for normal M giants and carbon stars, the Balmer lines are seen in absorption. For each panel a cut at

$$EW(\text{Strongest Balmer}) < -1\text{\AA}, \quad (12)$$

was adopted. We were thus left with 937 O-rich and 263 C-rich candidates, which were subsequently inspected by eye.

4.5. By-Eye Inspection

By-eye inspection can help us to decide whether a negative EW value represents real emission or just spectral noise. The major difficulty resides in identifying C-rich Mira spectra, because for normal C-rich stars of N spectral type, $H\alpha$ tends to be filled in or weak in emission. We rejected spectra with deep $\text{CaII } \lambda\lambda 8498, 8542, 8662$ absorption features (Section 3.3). In addition, we tried to make sure that all selected C-rich spectra exhibited strong $H\alpha$ or $H\beta$ emission. The 199 spectra identified in this step are shown in the Appendix (see Figures 13 and 14).

We have summarized the full selection process in Table 3. Our final sample of 191 identified Mira variables is provided in Table 4.

4.6. Spatial Distribution

Figure 9 shows the spatial distribution of the newly identified Mira candidates in Galactic coordinates. Among the 2724 AAVSO Miras with available SIMBAD subtypes, the C- to O-rich ratio is only 0.13.⁷ As regards the 191 Miras identified using LAMOST, this ratio increases to 0.74. This difference might be the result of a

⁷ We did not include S stars, because they can be either O- or C-rich, and the total fraction of S-type Miras is small.

TABLE 3
STEPS TO IDENTIFY MIRA STARS

Step	Criteria	O-rich	C-rich	Total # candidates
1	$SNR(i) > 20$			5,025,780
2	LAMOST Pipeline subclass	311,867	2184	314,051
3	+ Previously identified N-type star	311,867	2314	314,181
4	– Known Mira spectra	311,537	2273	313,810
3	$J - K_s > 1$ mag, $K_s < 12$ mag	31,795	762	32,557
4	– SIMBAD type: not a Mira	30,738	755	31,493
5	Eqs (7), (8)	21,989	755	22,744
6	Eq. (11)	21,651(+14)	755	20,542
7	Eq. (12)	937(+14)	263	1214
8	Inspection by eye	106(+14)	93	213
9	Single epoch	110	81	191

TABLE 4
MIRA STARS DISCOVERED IN LAMOST DR4

R.A. (J2000) degree	Dec. (J2000) degree	Designation	Epoch ^a	SIMBAD ^b	J mag	H mag	K_s mag	σ_J ^c mag	σ_H mag	σ_{K_s} mag	SpType ^d
30.03712	41.62985	J020008.90+413747.4	56256	C*	10.867	9.549	8.656	0.024	0.003	0.02	Carbon
301.53141	46.14646	J200607.53+460847.2	56560 57298 ^e	C*	8.85	7.803	7.327	0.029	0.026	0.023	Carbon
78.49842	30.11585	J051359.62+300657.0	55858 55909		8.902	7.931	7.44	0.026	0.026	0.02	M5, M4 ^f
15.59558	37.91861	J010222.93+375506.9	55907	LPV*	7.432	6.546	6.16	0.03	0.029	0.02	M7
93.02157	12.11717	J061205.17+120701.8	57388	IR	7.291	5.999	5.195	0.023	0.034	0.018	M8

NOTE. — This table is available in its entirety in machine-readable form.

^a LAMOST Modified Julian Day (MJD).

^b SIMBAD main type.

^c 2MASS photometric uncertainty.

^d Spectral subtype.

^e LAMOST observed this target twice.

^f Temperature type of different observations.

difference between the spatial distributions of the different types of AGB stars. It has been reported that O-rich AGB stars are concentrated toward the Galactic Center, whereas C-rich AGB stars exhibit a relatively uniform distribution (Ishihara et al. 2011), including a few C-rich Miras recently confirmed in the bulge (Matsunaga et al. 2017). Since the target selection of the LAMOST survey is not spatially uniform, but has a concentration of stars in the Galactic Anticenter direction (Deng et al. 2012; Liu et al. 2014), our selected Miras contain larger numbers of carbon stars, and they are thus distributed more commonly toward the $l \sim 180^\circ$ region.

5. DISCUSSION AND CONCLUSION

In this work, we have carefully studied 291 LAMOST spectra of known Mira stars to explore the optical properties of Miras. For O-rich stars, a relationship between the relative Balmer emission-line strength and spectral temperature is clearly shown. The $F_{H\delta}/F_{H\gamma}$ emission-line flux ratio increases as stars cool down from M0 to M10. Spectra earlier than M4 exhibit stronger $H\gamma$ than $H\delta$, which is a new result reported here. This relation can be explained by overlying TiO molecular-band absorption affecting lower-order Balmer lines. Metallic emission of Fe I $\lambda\lambda 4202, 4308, 4376$ and Mg I $\lambda 4571$ is only observed in late-type stars.

Based on the well-established relation between Balmer emission-line strength and the corresponding pulsation phase, our result shows that such a relation is indeed a population property exhibited by Mira variables. Future LAMOST observations can place stronger constraints on the rise duration and maximum phase of $H\delta$ and $H\gamma$ for

O-rich Miras.

Based on the characteristics of the 291 spectral templates, we identified 191 Mira candidates in the LAMOST DR4 catalog. Our criteria to select Mira stars make the most of a wide variety of available data (AAVSO VSX, SIMBAD, KISOGP, 2MASS, pipeline subclasses, spectral flux), and this is thus an efficient approach in terms of time commitment. Meanwhile, we made sure that every rejection was carefully assessed and that inaccurate measurements were not used. In terms of completeness, if we apply our the method outlined in Section 4, 135 of the 291 template spectra we studied in Section 3 can be selected. About half of the templates are rejected based on spectroscopic (null emission at a given phase) or photometric (bluer than the bulk of other Miras) criteria. Therefore, we estimate that the DR4 catalog may include a total of $191 \times \frac{291}{135} \simeq 412$ new Miras, with some $412 - 191 = 221$ remaining undetected.

Note that since Mira variables are defined by their luminosity variability, photometric observations are required to further confirm that the newly identified candidates are bona fide Mira stars. It is worth noting that six candidates have good photometric data and are located within the KISOGP field. The light curves of three candidates look like Miras (and all of them show long-term trends); two are found near the boundary between Miras and semi-regular variables, while the other is probably not a Mira. From this analysis we conservatively expect the ratio of bona fide Mira stars to the number of selected candidates to exceed 50%.

Newly discovered Mira candidates should usefully contribute to studies of stellar evolution of late-type stars

(especially to shock-induced pulsation studies of C-rich stars) in the Galactic Anticenter. Eight of the 111 O-rich candidates are of type M0–M2, which are rare cases. This speaks volumes for LAMOST’s ability to capture the spectra of early-type Miras through such a ‘treasure hunt’. Also, at least 24 of the 191 Miras are located in the Galactic halo (Galactic latitude $> 30^\circ$) and can possibly be used as tracers of stellar streams, although their low space density may prevent us from investigating small structures.

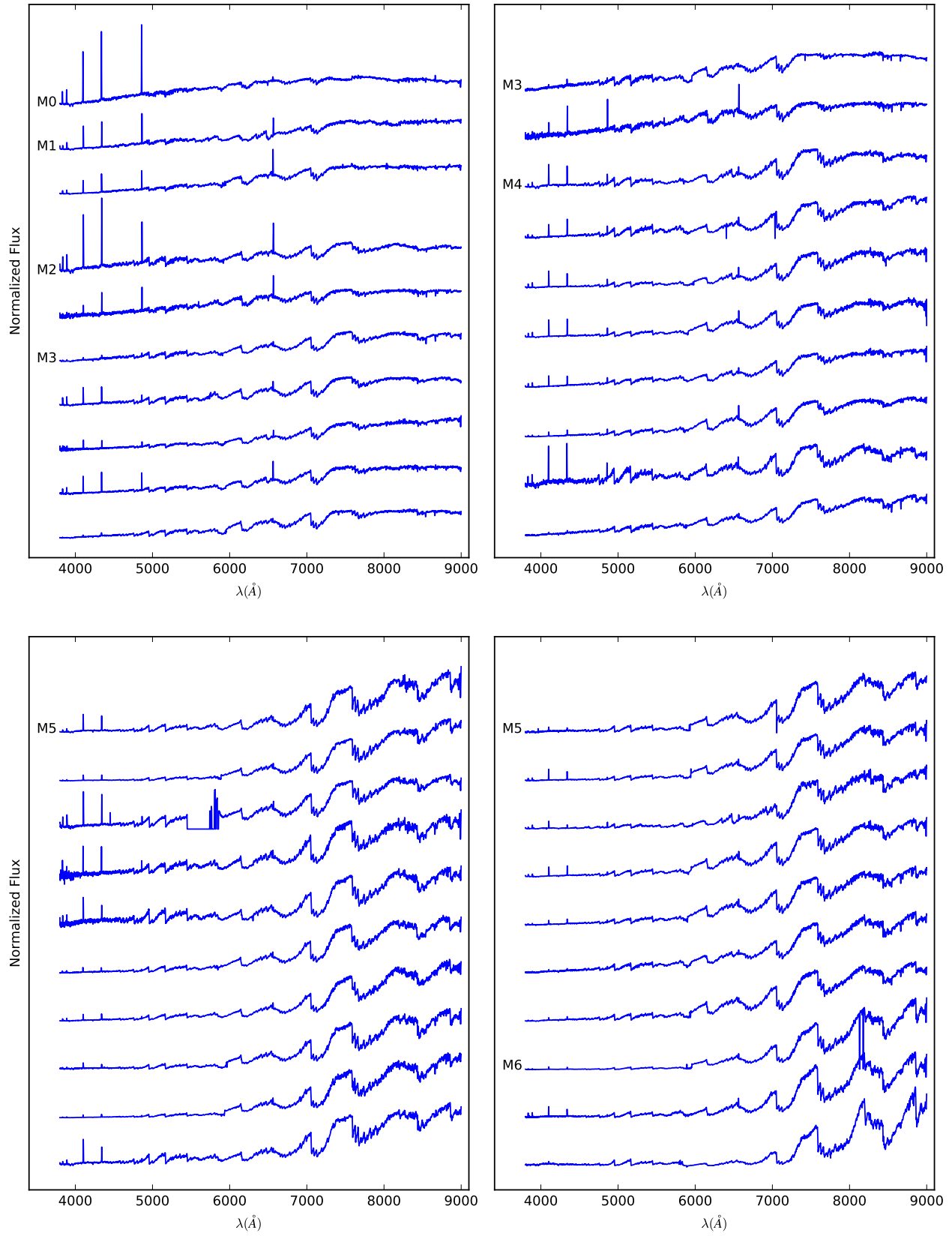
We acknowledge with pleasure the anonymous reviewer who has offered valuable suggestions. This work was supported by the Hui-Chun Chin and Tsung-Dao Lee Chi-

nese Undergraduate Research Endowment (CURE). C.L. acknowledges support from both the National Key Basic Research Program of China (grant 2014CB845700) and the National Natural Science Foundation of China (NSFC; grants 11373032 and 11333003). R.d.G. acknowledges NSFC funding through grants U1631102, 11373010, and 11633005. The Guoshoujing Telescope (the Large Sky Area Multi-Object Fiber Spectroscopic Telescope, LAMOST) is a National Major Scientific Project constructed by the Chinese Academy of Sciences. Funding for the project was provided by the National Development and Reform Commission. LAMOST is operated and managed by the National Astronomical Observatories, Chinese Academy of Sciences.

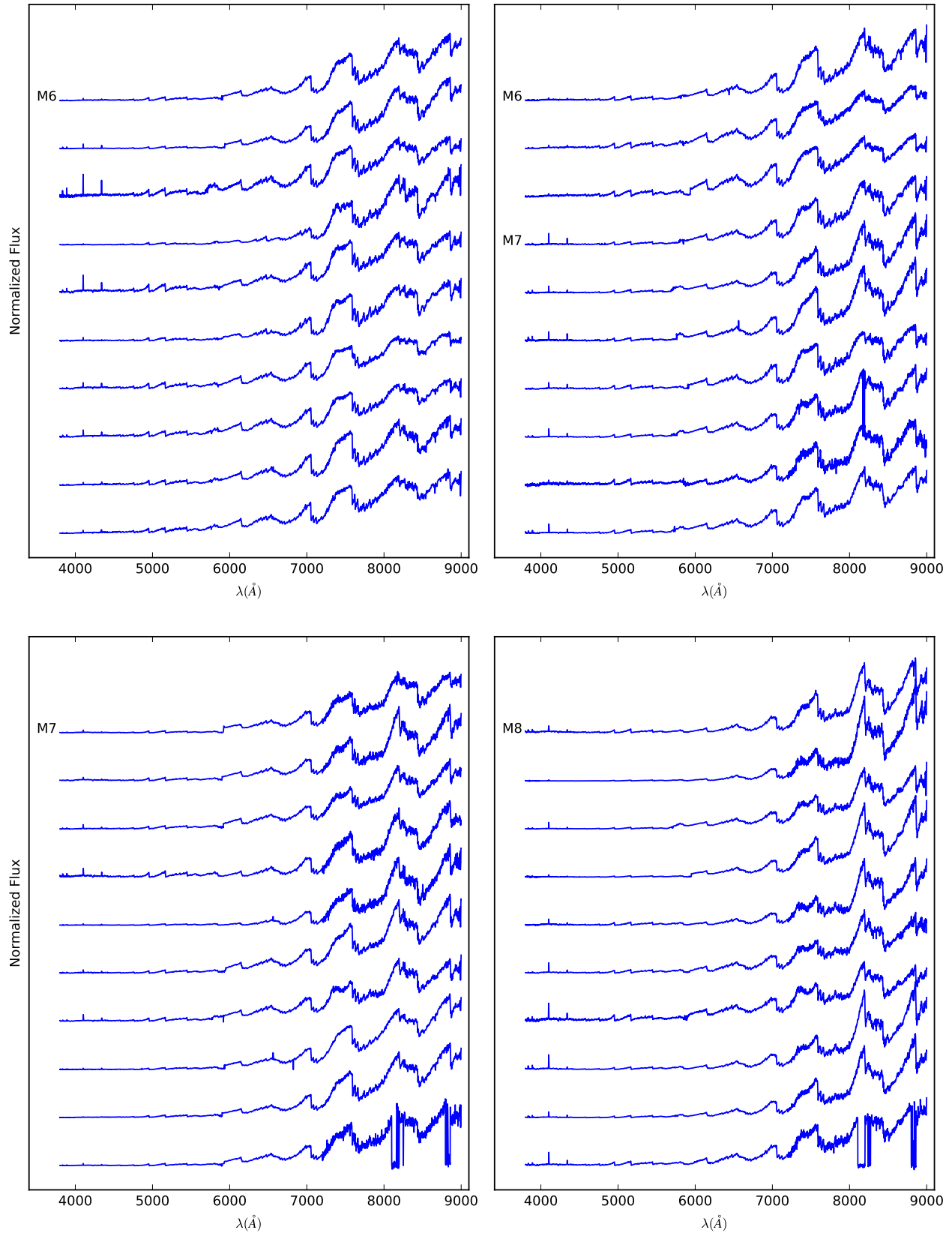
REFERENCES

- Adams, W. S. 1941, *ApJ*, 93, 11
 Barnbaum, C., Stone, R. P. S., & Keenan, P. C. 1996, *ApJS*, 105, 419
 Bowen, G. H. 1988, *ApJ*, 329, 299
 Castelaz, M. W., Luttermoser, D. G., Caton, D. B., & Piontek, R. A. 2000, *AJ*, 120, 2627
 Catchpole, R. M., Whitelock, P. A., Feast, M. W., et al. 2016, *MNRAS*, 455, 2216
 Cui, X.-Q., Zhao, Y.-H., Chu, Y.-Q., et al. 2012, *RAA*, 12, 1197
 Deason, A. J., Belokurov, V., Erkal, D., Koposov, S. E., & Mackey, D. 2017, *MNRAS*, 467, 2636
 de Grijs, R. 2011, *An Introduction to Distance Measurement in Astronomy*, Wiley Acad. Publ.
 Deguchi, S., Fujii, T., Ita, Y., et al. 2007, *PASJ*, 59, 559
 Deguchi, S., Fujii, T., Ita, Y., et al. 2008, *Astrophys. Space Sci. Proc.*, 4, 33
 Deguchi, S., Shimoikura, T., & Koike, K. 2010, *PASJ*, 62, 525
 Deguchi, S. 2012, *Cosmic Masers – from OH to H₀*, *IAU Symp.*, 287, p. 265
 de Laverny, F., & Magnan, C. 1995, *IAU Colloq. 155: Astrophysical Applications of Stellar Pulsation*, 83, 419
 Deng, L.-C., Newberg, H. J., Liu, C., et al. 2012, *RAA*, 12, 735
 Deutsch, A. J., & Merrill, P. W. 1959, *ApJ*, 130, 570
 Fadeyev, Y. A., & Gillet, D. 2004, *A&A*, 420, 423
 Fluks, M. A., Plez, B., The, P. S., et al. 1994, *A&AS*, 105,
 Fox, M. W., Wood, P. R., & Dopita, M. A. 1984, *ApJ*, 286, 337
 Fox, M. W., & Wood, P. R. 1985, *ApJ*, 297, 455
 Fujii, T., Deguchi, S., Ita, Y., et al. 2006, *PASJ*, 58, 529
 Giridhar, S. 2010, *Bull. Astron. Soc. India*, 38, 1
 Gorbatskii, V. G. 1961, *Soviet Ast.*, 5, 192
 Gray, R. O., & Corbally, C., J. 2009, *Stellar Spectral Classification*, Princeton, NJ: Princeton Univ. Press
 Green, P. 2013, *ApJ*, 765, 12
 Habing, H. J., & Olofsson, H. 2003, *Asymptotic giant branch stars*, New York, Berlin: Springer
 Herczeg, G. J., & Hillenbrand, L. A. 2014, *ApJ*, 786, 97
 Ishihara, D., Kaneda, H., Onaka, T., et al. 2011, *A&A*, 534, A79
 Ji, W., Cui, W., Liu, C., et al. 2016, *ApJS*, 226, 1
 Joy, A. H. 1947, *ApJ*, 106, 288
 Joy, A. H. 1954, *ApJS*, 1, 39
 Keenan, P. C., & Boeshaar, P. C. 1980, *ApJS*, 43, 379
 Liu, C., Cui, W.-Y., Zhang, B., et al. 2015, *RAA*, 15, 1137
 Liu, X.-W., Yuan, H.-B., Huo, Z.-Y., et al. 2014, *Setting the scene for Gaia and LAMOST*, 298, 310
 López-Corredoira, M. 2017, *ApJ*, 836, 218
 Luo, A.-L., Zhang, H.-T., Zhao, Y.-H., et al. 2012, *RAA*, 12, 1243
 Luo, A.-L., Zhao, Y.-H., Zhao, G., et al. 2015, *RAA*, 15, 1095
 Luttermoser, D. G., & Bowen, G. H. 1992, *Cool Stars, Stellar Systems, and the Sun*, Giampapa, M. S., & Bookbinder, J. A., eds, *ASP Conf. Ser.*, 26, 558
 Mann, A. W., Gaidos, E., Lépine, S., & Hilton, E. J. 2012, *ApJ*, 753, 90
 Marigo, P., Girardi, L., Bressan, A., et al. 2008, *A&A*, 482, 883
 Matsunaga, N., Kawadu, T., Nishiyama, S., et al. 2009, *MNRAS*, 399, 1709
 Matsunaga, N. 2017, *arXiv:1705.08567*
 Matsunaga, N., Menzies, J. W., Feast, M. W., et al. 2017, *MNRAS*, 469, 4949
 Merrill, P. W. 1940, *Spectra of long-period variable stars*, Chicago, IL: Univ. Chicago Press
 Merrill, P. W. 1945, *PASP*, 57, 178
 Mikulášek, Z., & Gráf, T. 2005, *Contrib. Astron. Obs. Skalnaté Pleso*, 35, 83
 Neilson, H. R., Ignace, R., & Henson, G. D. 2014, *Precision Asteroeismology*, Guzik, J. A., Chaplin, W. J., Handler, G., & Pigulski, A., eds, *IAU Symp.*, 301, 463
 Osterbrock, D. E. 1974, *Astrophysics of gaseous nebulae*, San Francisco, CA: W. H. Freeman and Co.
 Pojmański, G. 2014, *Contrib. Astron. Obs. Skalnaté Pleso*, 43, 523
 Reid, I. N., Hawley, S. L., & Gizis, J. E. 1995, *AJ*, 110, 1838
 Rejkuba, M. 2004, *A&A*, 413, 903
 Richter, H., Wood, P. R., Woitke, P., Bolick, U., & Sedlmayr, E. 2003, *A&A*, 400, 319
 Richter, H., & Wood, P. R. 2001, *A&A*, 369, 1027
 Saffe, C., Gómez, M., Randich, S., et al. 2003, *A&A*, 409, 993
 Scalo, J. M., & Ross, J. E. 1976, *A&A*, 48, 219
 Siviero, A., Munari, U., Righetti, G. L., & Graziani, M. 2016, *Inf. Bull. Variable Stars*, 6183, 1
 Skrutskie, M. F., Cutri, R. M., Stiening, R., et al. 2006, *AJ*, 131, 1163
 Van Eck, S., Neyskens, P., Jorissen, A., et al. 2017, *A&A*, 601, A10
 Watson, C. L. 2006, *Soc. Astron. Sci. Annu. Symp.*, 25, 47
 Whitelock, P. A., Feast, M. W., & van Leeuwen, F. 2008, *MNRAS*, 386, 313
 Whitelock, P. A. 2013, *Advancing the Physics of Cosmic Distances*, *IAU Symp.*, 289, 209
 Willson, L. A. 1976, *ApJ*, 205, 172
 Wiśniewski, M., Marquette, J. B., Beaulieu, J. P., et al. 2011, *A&A*, 530, A8
 Woźniak, P. R., Vestrand, W. T., Akerlof, C. W., et al. 2004, *AJ*, 127, 2436
 Worthey, G., Faber, S. M., Gonzalez, J. J., & Burstein, D. 1994, *ApJS*, 94, 687
 Zechmeister, M., & Kürster, M. 2009, *A&A*, 496, 577
 Zhao, G., Zhao, Y.-H., Chu, Y.-Q., Jing, Y.-P., & Deng, L.-C. 2012, *RAA*, 12, 723
 Zhong, J., Lépine, S., Li, J., et al. 2015, *RAA*, 15, 1154

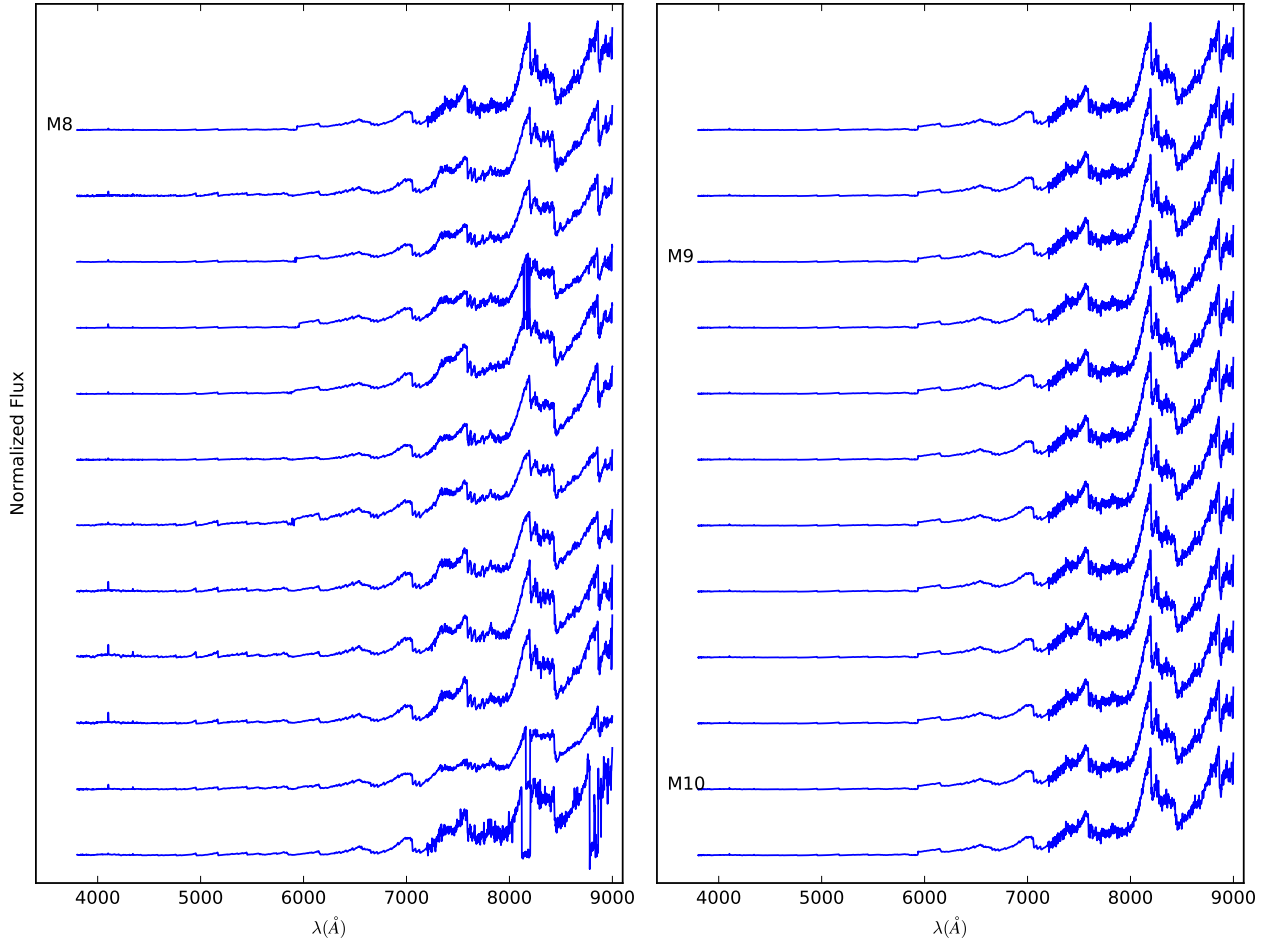
APPENDIX



(a)

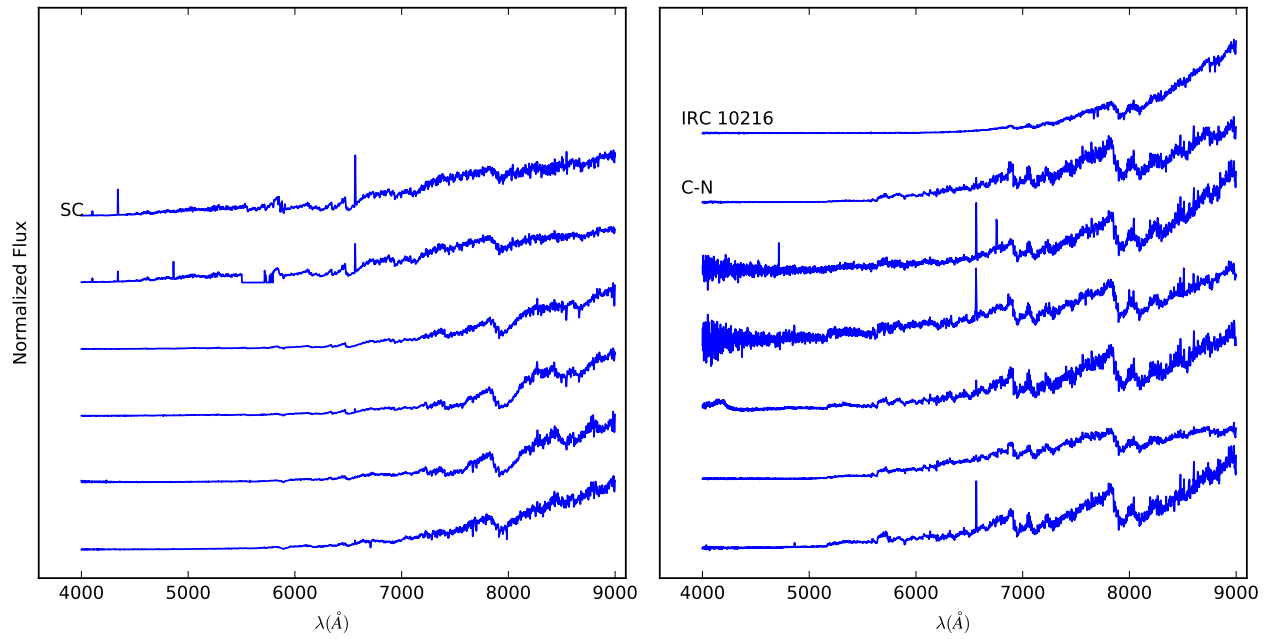


(b)



(c)

FIG. 10.— Spectra of O-rich Mira templates, only uncorrupted spectra with emission lines are shown.



(a)

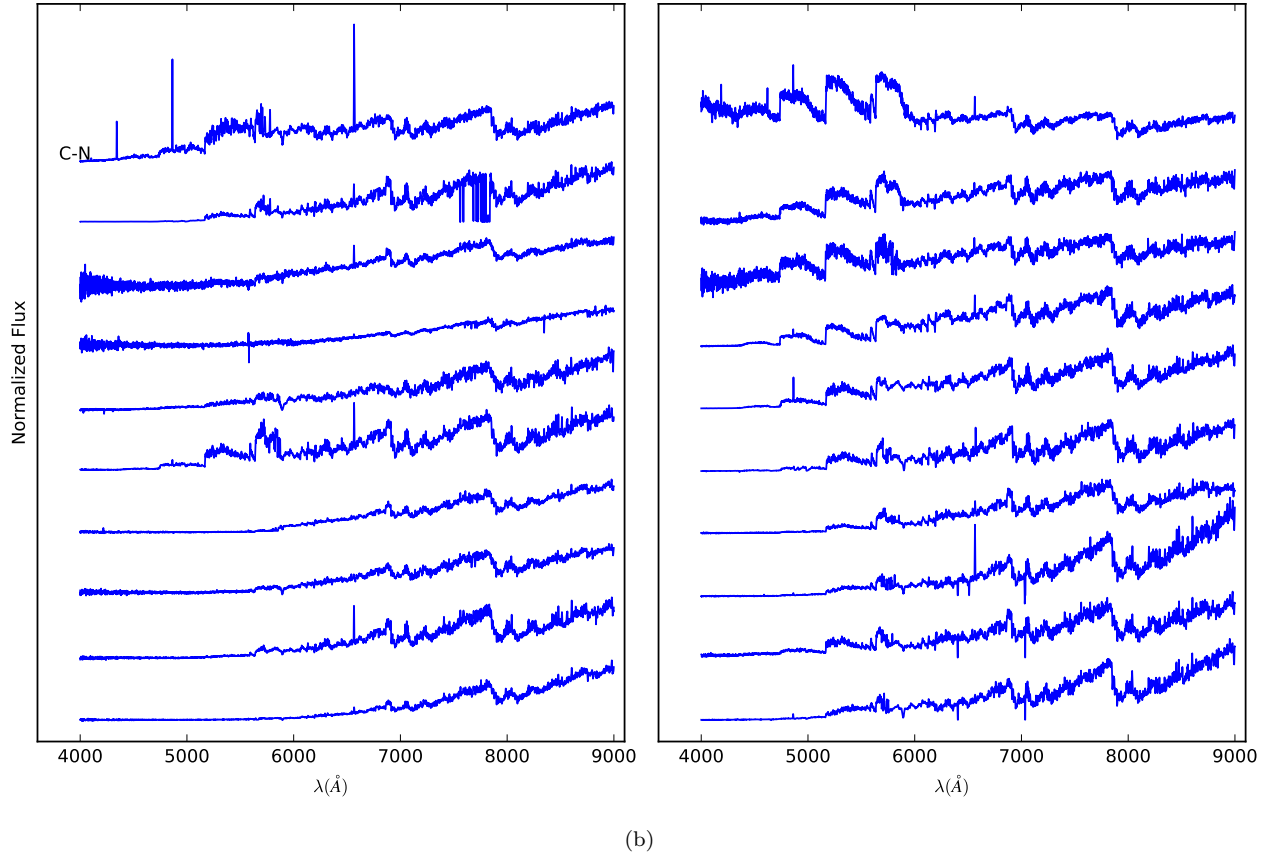


FIG. 11.— Spectra of C-rich Mira candidates. The widely studied carbon star IRC 10216 is marked because of its redness.

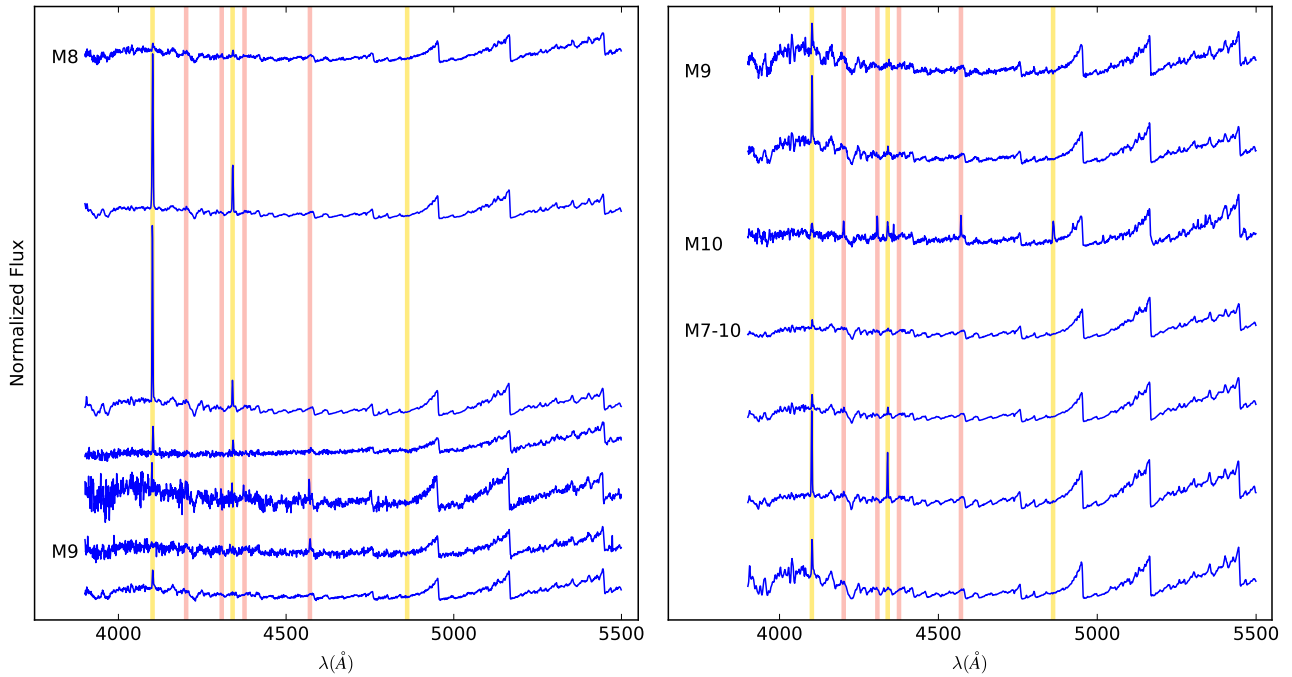
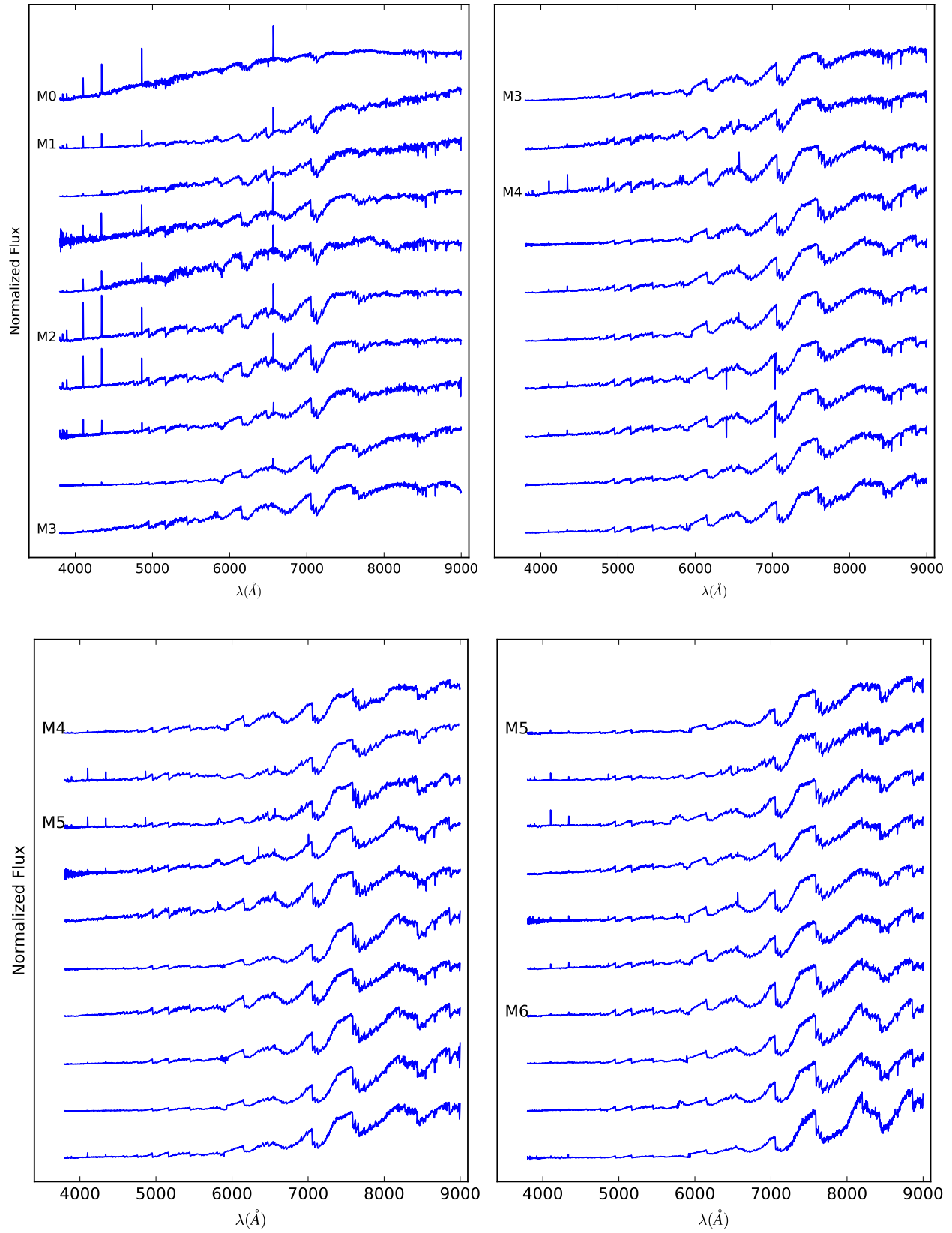
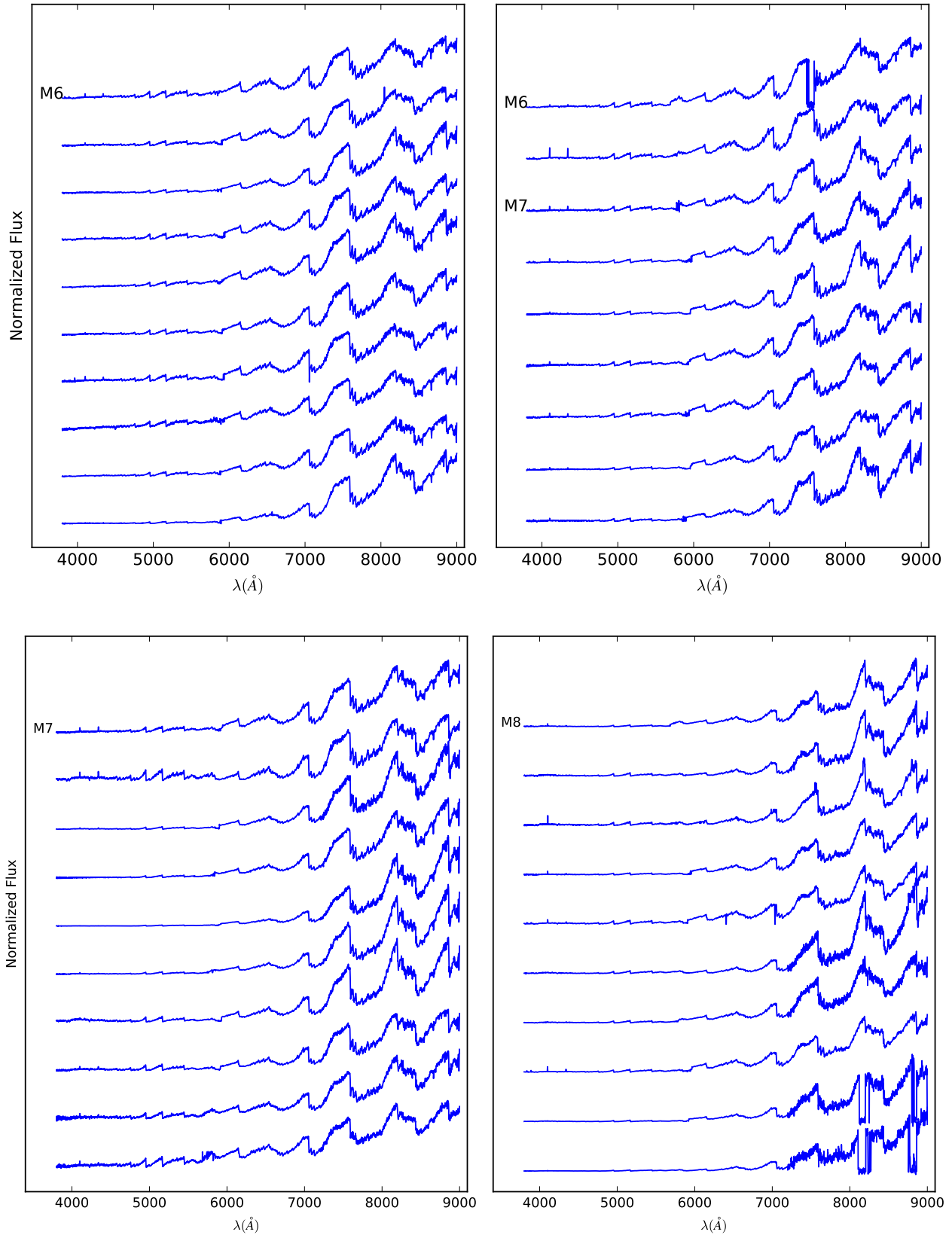


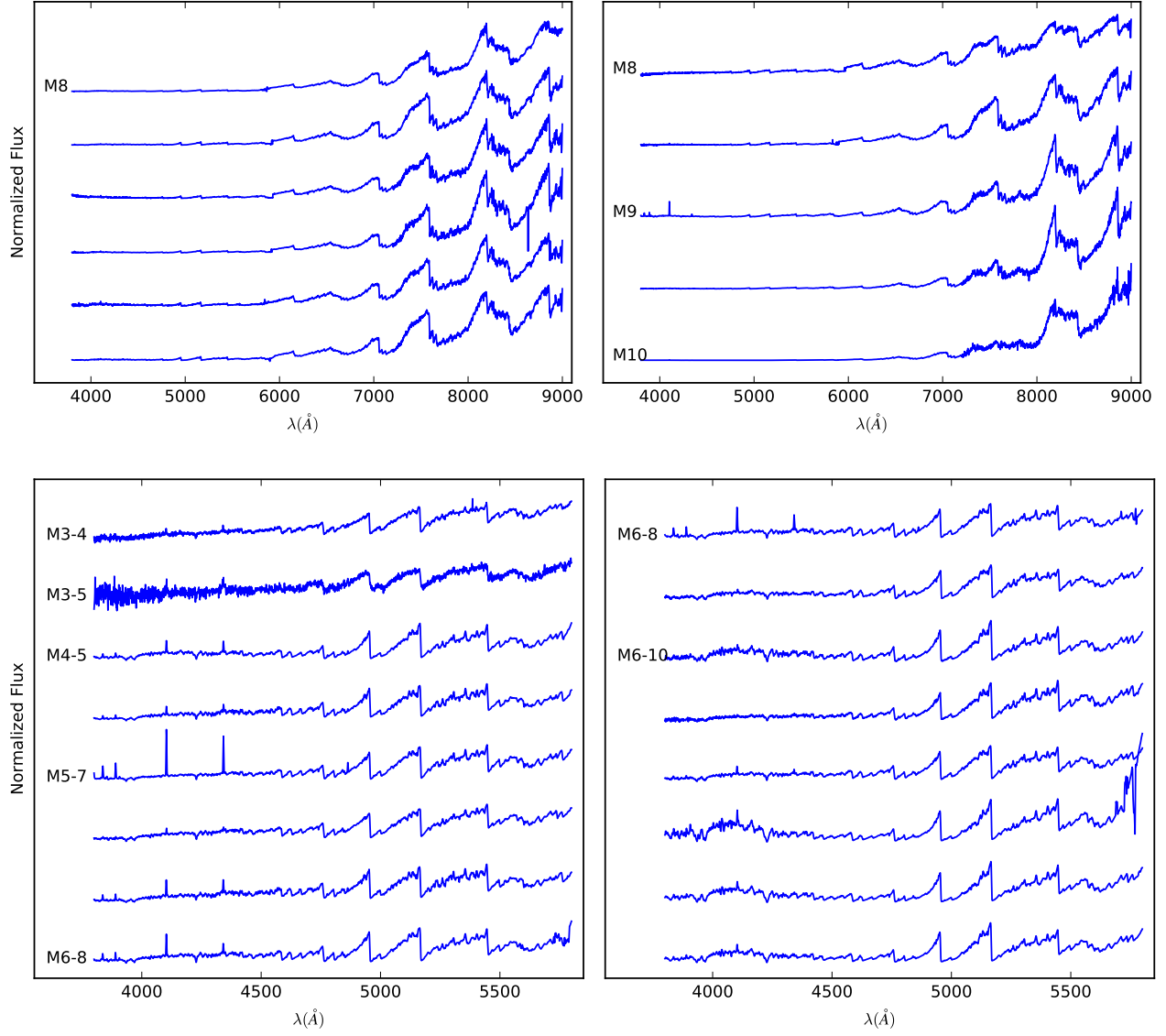
FIG. 12.— Spectra selected in Section 4.3. Temperature types of four spectra can only be roughly determined as M7–M10, because their red sections suffer from saturation.



(a)

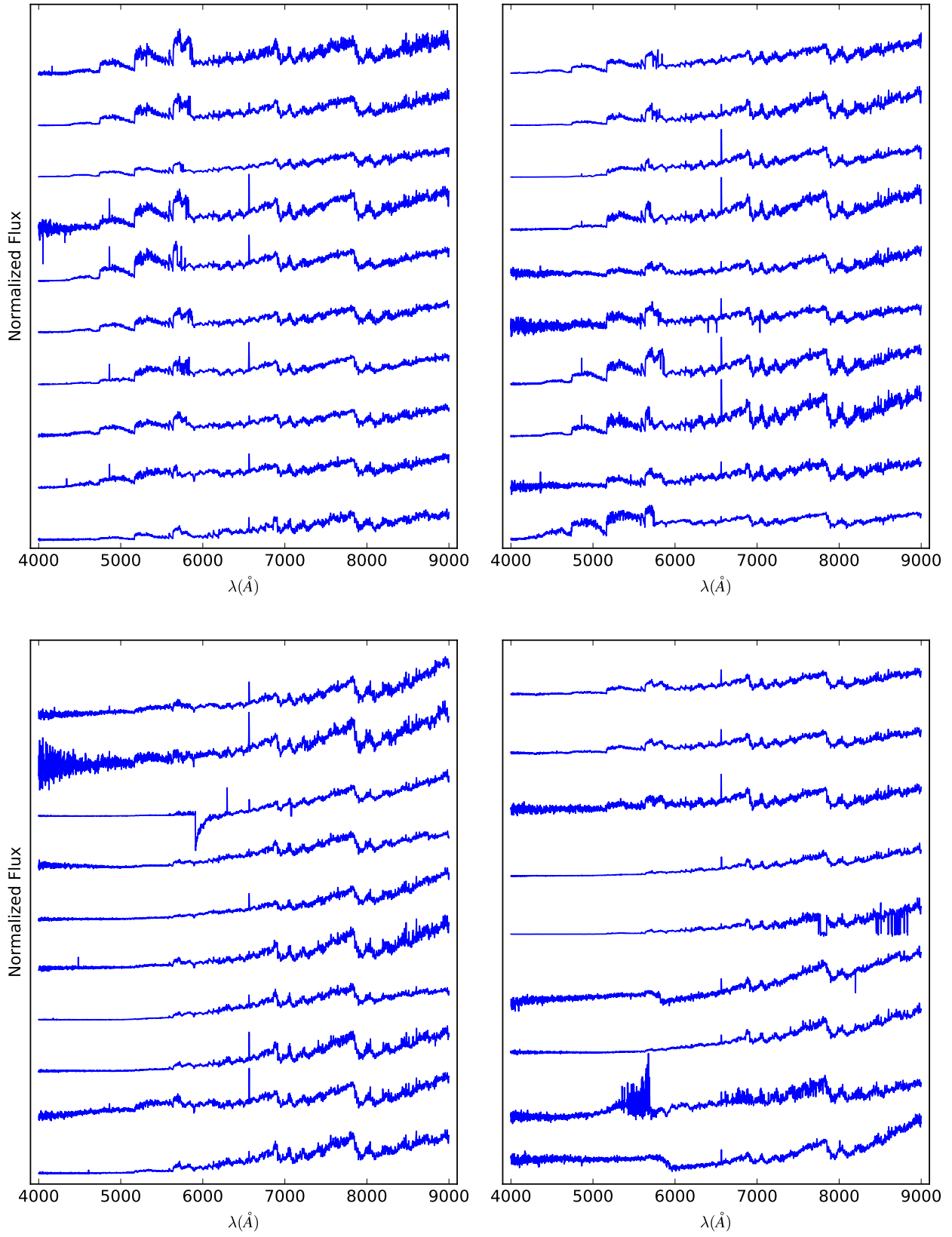


(b)

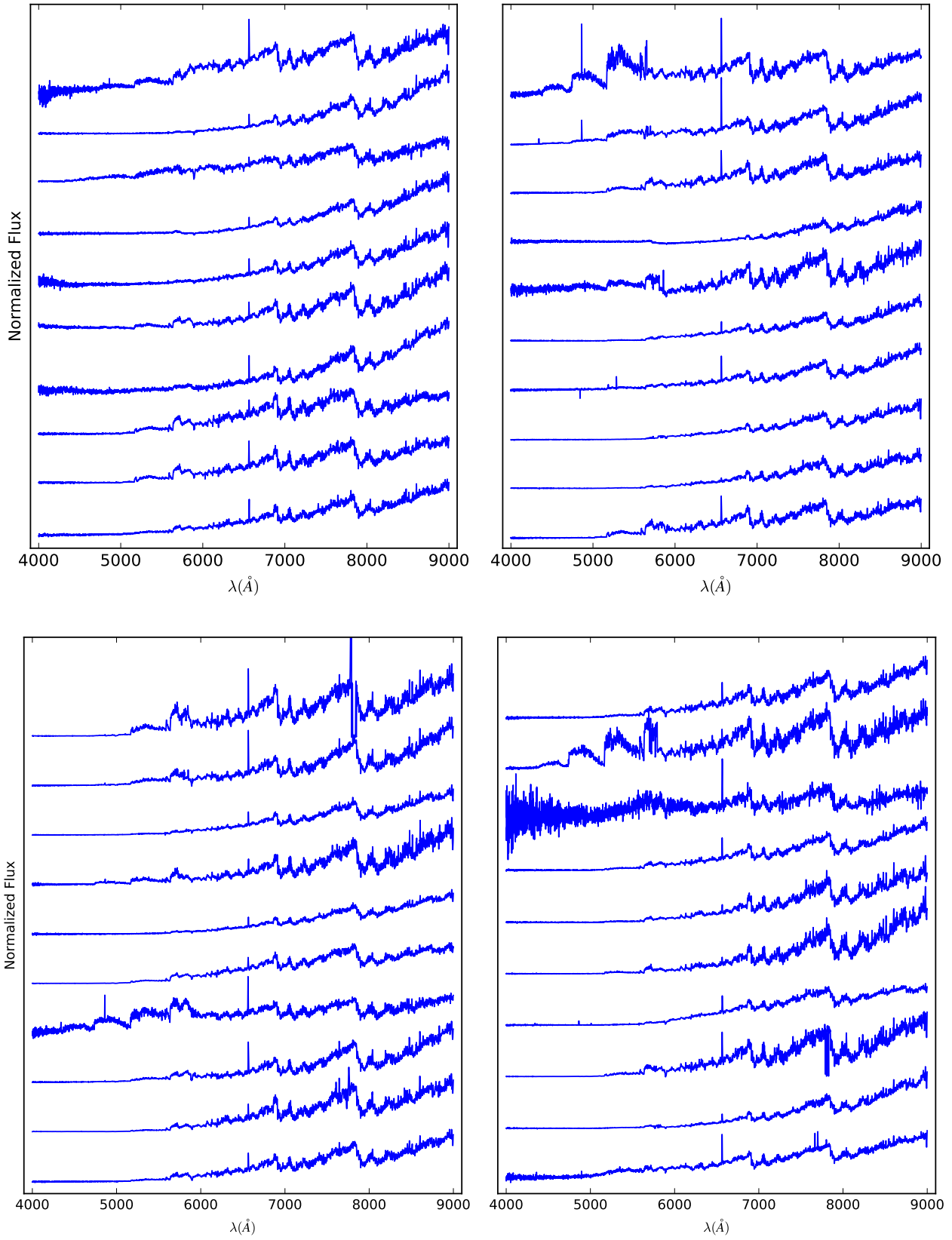


(c)

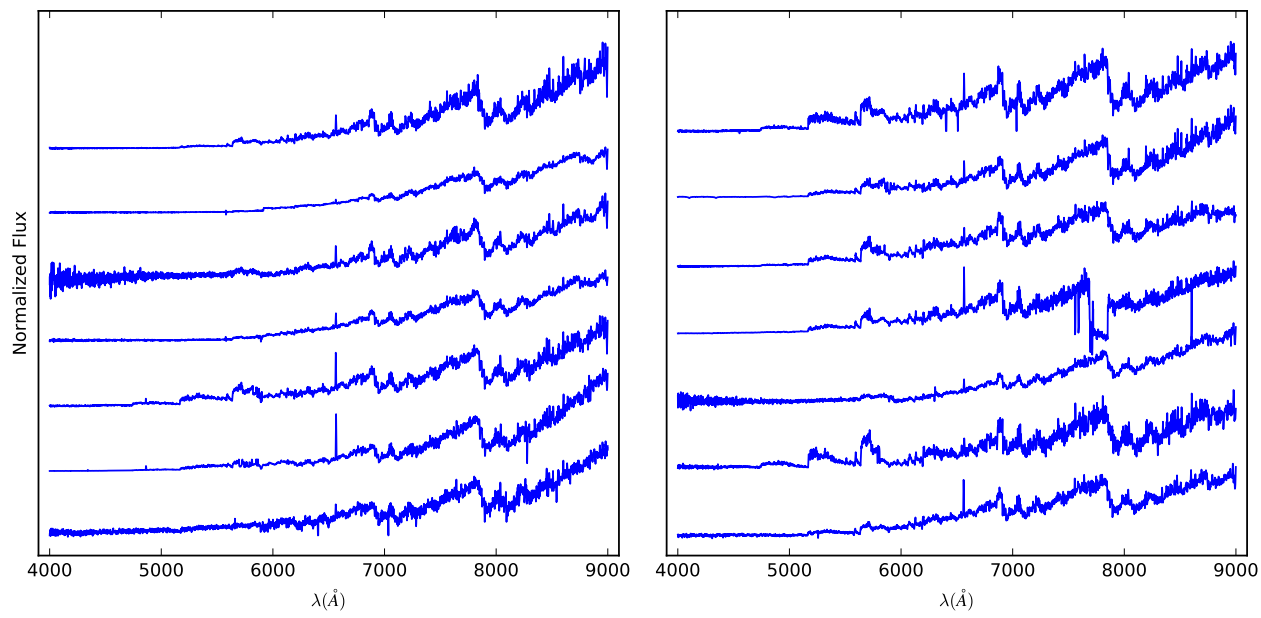
FIG. 13.— O-rich Mira candidate spectra selected in Section 4.5 from LAMOST DR4. Temperature types of 16 of them can only be roughly determined because of long-wavelength saturation.



(a)



(b)



(c)

FIG. 14.— C-rich Mira candidate spectra selected in Section 4.5 from LAMOST DR4.